Third-order nonlinear optical spectroscopy in CuCl†

S. D. Kramer* and N. Bloembergen
Gordon McKay Laboratory, Harvard University, Cambridge, Massachusetts 02138
(Received 7 May 1976)

The production of light at the combination frequency $2\omega_1$-ω_2 by two incident-tunable coherent beams at the frequencies ω_1 and ω_2, respectively, has been studied in CuCl, as $2\omega_1$ is varied across the Z_3-exciton-polariton dispersion curve, and/or $\omega_1 - \omega_2$ is varied across the longitudinal phonon-polariton dispersion curve. The interference of the excitonic and Raman resonances with the nonresonant electronic nonlinear susceptibility gives new information about the nonlinear properties of the Z_3 exciton and its damping as a function of temperature. A detailed theoretical and experimental comparison with earlier work on two-photon absorption and second-harmonic generation in CuCl is presented.

I. INTRODUCTION

The pioneering work of Maker and Terhune[1] in creating radiation at the anti-Stokes frequency $2\omega_1 - \omega_2$ by two light beams, with a difference in frequency $\omega_1 - \omega_2$ close to a vibrational resonance of a molecule, has been followed in recent years by extensive investigations of the generation of combination frequencies. The systematic study of the frequency dependence of third-order nonlinearities has been made possible by the availability of tunable coherent beams. Dye lasers can cover nearly continuously the region of the near ultraviolet to the near infrared, from about 0.3 to 1.1 μm wavelength. Parametric oscillators may be used to generate tunable radiation farther in the infrared. The generation of the combination frequency $2\omega_1 - \omega_2$ is particularly attractive because it permits the study of dispersive properties near the intermediate frequencies $2\omega_1$ and $\omega_1 - \omega_2$. These may typically lie in highly absorbing ultraviolet and infrared regions of the spectrum, while the light beams at ω_1, ω_2, and $\omega_3 = 2\omega_1 - \omega_2$ all lie in the transparent region of the material being investigated.

Alkali and earth-alkali-metal vapors and centrosymmetric crystals have been extensively studied using this technique.[2] This work has been summarized in several recent review papers.[3-5] The relevant theory in noncentrosymmetric crystals has also been reviewed.[6]

The present paper presents a comprehensive study of the generation of radiation at $2\omega_1 - \omega_2$ by three-wave mixing in the noncentrosymmetric cubic crystal CuCl which has $\bar{4}3m$ symmetry. Some preliminary results have been reported earlier.[7]

Cuprous chloride at liquid-helium temperature shows a sharp excitonic structure which has been studied extensively by linear spectroscopy.[8-12] Cardona[13] has pointed out that CuCl is the only known zinc-blende-type semiconductor with a nondegenerate highest valence band at the center of the Brillouin zone. The lowest exciton level is consequently a particularly sharp Z_3 excitation. At 4.2 °K this Z_3 exciton causes a sharp absorption line near 3860 Å, with a linear absorption depth of about 3×10^{-6} cm. As a result the high-absorption linear spectroscopy must be carried out in very thin films[8-10] or by reflection techniques.[12] In either case only excitons close to a surface are probed. Their properties may be altered by physical and chemical contamination of the surface to which CuCl is particularly vulnerable.

Since the CuCl structure lacks inversion symmetry, the Z_3-exciton polariton contributes a resonant term in second-harmonic generation if the incident photon energy is at half the exciton energy.[14] Unfortunately, this method is extremely sensitive through the phase-matching condition to the linear index of refraction which varies markedly near a material resonance. This makes the interpretation of the experimental results less than straightforward. In addition, as in the linear studies only excitons near a surface can be studied. In contrast, in two-photon absorption experiments[15,16] which are a form of third-order spectroscopy the excitons can be created in the bulk volume of the crystal. The resulting excitation can then be detected by fluorescent recombination or through the attenuation of the incident beams.

Theory[6] predicts a close relationship between processes at $2\omega_1$, induced by one or two incident light beams at ω_1, and the frequency mixing induced by light beams at frequencies ω_1 and ω_2, respectively. The three-wave mixing experiments involve only light beams in the relatively nondispersive transparent region of the crystal. The phase-matching condition is only weakly dependent on frequency. The exciton can be probed in the bulk volume with high sensitivity, and this method can augment the information about exciton properties found in lower-order studies in a significant way.

The general features of the effective third-order nonlinear susceptibility in noncentrosymmetric crystals[6] may be tested in the simple $\bar{4}3m$ symmetry. In addition to direct third-order mixing there are contributions by a two-step process proportional to $(\chi^{(2)}_{xyz})^2$. The sharp exciton resonance at $2\omega_1$ provides the opportunity to see the interference effects between this resonance and the nonresonant nonlinearity of electronic states in the conduction bands. Previously, sharp two-photon resonant contributions have been observed in alkali vapors, but for these the nonresonant contribution is negligible and so no interference is seen. Broad features of a two-photon absorption contribution to the light-mixing process have been reported by Levenson and Bloembergen[2] in diamond and some organic liquids, but these would not permit the observation of typical interference patterns. Contributions of the Raman resonance of the phonon-polariton infrared excitation at $\omega_1 - \omega_2$ can be observed simultaneously with those of the exciton resonance at $2\omega_1$. The interference effects of the exciton and phonon polariton with each other and with the nonresonant nonlinearity, briefly reported in a short communication,[17] are discussed in detail.

A review of the general theoretical framework of third-order nonlinear spectroscopy will be given in Sec. II. The experimental arrangement used in this study will be described in Sec. III, and in Sec. IV the experimental results will be presented. Their analysis yields new data on both the linear and nonlinear properties of cuprous chloride and its exciton and phonon-polariton excitations. More details than could be incorporated in this paper can be found in an unpublished doctoral dissertation by the first author.[18]

II. REVIEW OF NONLINEAR RESPONSE THEORY OF EXCITONS

The theory of the nonlinear response of excitonic polaritons is formally quite similar to the theory for phonon polaritons which was developed earlier. Among others, Flytzanis and Bloembergen[6] and Boggett and Loudon[19,20] have reviewed the nonlinear response of polariton excitations and have obtained essentially identical results. The general formulation of Flytzanis and Bloembergen[6] and Yablonovitch *et al.*[21] is used here to introduce the subject. A generalized exciton coordinate Q describes the excitonic degree of freedom and is separated from all other electronic states. This procedure is useful if a single excitation is near resonance and its resonance effects on the linear and nonlinear electromagnetic response are to be analyzed. The contributions of all other electronic degrees of freedom are lumped together in nonresonant linear and nonlinear susceptibilities. The Hamiltonian is developed in an ascending double-power series in the exciton coordinate Q and the macroscopic electric field E:

$$\begin{aligned}\mathcal{H} = &(-Ne^*EQ + \tfrac{1}{2}NM\omega_T^2Q^2 - \tfrac{1}{2}\chi^{(1)}E^2)\\ &+(-\tfrac{1}{3}\chi^{(2)}E^3 + N\zeta^{(2)}\tfrac{1}{3}Q^3 - \tfrac{1}{2}N\alpha_T E^2Q - N\gamma^{(2)}EQ^2)\\ &+(-\tfrac{1}{3}N\beta_1^{(3)}E^3Q - \tfrac{1}{2}N\beta_2^{(3)}E^2Q^2 - N\beta_3^{(3)}EQ^3\\ &+\tfrac{1}{4}N\zeta^{(3)}Q^4 - \tfrac{1}{4}\chi^{(3)}E^4). \qquad (1)\end{aligned}$$

In this expression e^* and M are the effective charge and reduced mass of exciton, respectively, while N is the electron volume density participating in the exciton formation. The transverse exciton resonant frequency is ω_T. For linear properties only the first bracketed term on the right-hand side needs to be retained. The other terms contain various nonlinear susceptibilities and coupling coefficients. Vector subscripts have been suppressed for clarity. The polarization, $P = \partial\mathcal{H}/\partial E$, derived from this Hamiltonian, contains the following first-, second-, and third-order terms:

$$\begin{aligned}P = &(Ne^*Q + \chi^{(1)}E) + (N\alpha_T EQ + N\gamma^{(2)}Q^2 + \chi^{(2)}E^2)\\ &+(N\beta_1^{(3)}E^2Q + N\beta_2^{(3)}EQ^2 + N\beta_3^{(3)}Q^3 + \chi^{(3)}E^3).\end{aligned} \qquad (2)$$

The force driving the exciton is given by $N^{-1}(-\partial\mathcal{H}/\partial Q)$ and the exciton equation of motion is described by an anharmonic oscillator equation,

$$\begin{aligned}M\ddot{Q} + M\Gamma\dot{Q} = &(-M\omega_T^2Q + e^*E)\\ &+(-\zeta^{(2)}Q^2 + \tfrac{1}{2}\alpha_T E^2 + 2\gamma^{(2)}EQ)\\ &+(\tfrac{1}{3}\beta_1^{(3)}E^3 + \beta_2^{(3)}E^2Q + 3\beta_3^{(3)}EQ^2 - \zeta^{(3)}Q^3).\end{aligned} \qquad (3)$$

Γ is a phenomenological damping constant. The electric field is related to the polarization by Maxwell's wave equation,

$$\nabla^2\vec{E} - \nabla(\nabla\cdot\vec{E}) - \frac{1}{c^2}\frac{\partial^2\vec{E}}{\partial t^2} = \frac{4\pi}{c^2}\frac{\partial^2\vec{P}}{\partial t^2}. \qquad (4)$$

The set of Eqs. (2)–(4) in E, P, and Q must be solved iteratively. If only linear terms, proportional to E and Q, are kept, linear exciton theory is recovered. When Q is eliminated, the linear relationship between P and E leads to the well-known dispersion characteristics shown in Fig. 1, where the units along the axes are appropriate for CuCl. In this crystal spatial dispersion effects are negligible. In the wave-vector range of interest there is no k dependence of the effective mass. The slope $d\omega/dk$ for an electromagnetic wave in the transparent region of the crystal, at about half the exciton energy shown, is also indicated in the

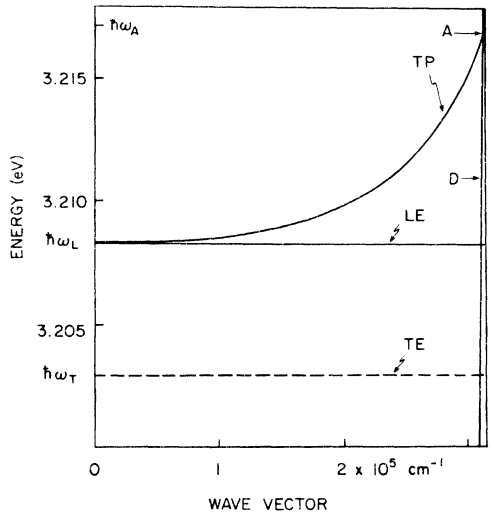

FIG. 1. Z_3-exciton dispersion relations in CuCl. The lower branch of the transverse exciton lies far to the right and is not shown in this picture. Only the horizontal asymptote TE is indicated. The nearly vertical line D has a slope ω_1/k_1, and the point of intersection A indicates the possibility of phase matching for forward waves in second-harmonic generation [after Fröhlich (Ref. 16)] TP denotes the upper transverse exciton-polariton branch and LE the longitudinal exciton branch.

figure by line D. The intersection point A indicates the possibility of phase matching for forward waves in second-harmonic generation on the upper transverse exciton-polariton curve. This is due to dispersive effects of higher excitonic levels and conduction bands. The lower transverse branch is far to the right of this line and is not shown in the figure. Only the horizontal asymptote for large k values, labeled TE, is shown. It occurs at the frequency $\omega = \omega_T$. Linear theory gives the dispersion relation

$$k^2 = \frac{\omega^2}{c^2}\left(\epsilon_\infty + \frac{4\pi N e^{*2}}{M(\omega_T^2 - \omega^2 - i\omega\Gamma)}\right). \tag{5}$$

As noted above, ϵ_∞ is not strictly a constant, but contains dispersion due to higher-energy levels. The complex index of refraction has been measured by Staude[12] and has been reproduced by Haueisen and Mahr.[14] The longitudinal exciton resonant frequency is given by the Lyddane-Teller-Sachs relation

$$\omega_L = \omega_T(\epsilon_0/\epsilon_\infty)^{1/2}. \tag{6}$$

ϵ_0 and ϵ_∞ are taken to be the dielectric constants in the dispersionless regions just below and above the exciton resonance.

If the procedure is iterated for the nonlinear terms in Eqs. (2)–(4) and the coordinate Q is again eliminated, one obtains to third order in the electric field the nonlinear polarization in the form

$$P^{\mathrm{NL}} = \chi^{(2)}_{\mathrm{eff}} EE + \chi^{(3)}_{\mathrm{eff}} EEE. \tag{7}$$

Here $\chi^{(2)}_{\mathrm{eff}}$ is the parameter of interest for second-harmonic generation, while the imaginary part of $\chi^{(3)}_{\mathrm{eff}}$ is proportional to the two-photon absorption signal. The intensity observed in a three-wave mixing experiment is proportional to $|\chi^{(3)}_{\mathrm{eff}}|^2$. Unfortunately, the solution for $\chi^{(3)}_{\mathrm{eff}}$ by the tedious iteration procedure contains 50 different terms.[6] Considerable simplification is possible, however, based on the fact that many terms do not have a resonant denominator and may consequently be combined in an effective nonresonant coefficient. This procedure will be illustrated for the second-order susceptibility. For two input waves at ω' and ω'', one finds that the polarization at the sum frequency is given by

$$\chi^{(2)}_{\mathrm{eff}}(-(\omega'+\omega''),\omega',\omega'') = [2-\delta(\omega'-\omega'')]\left(\frac{N}{2M}\frac{e^*\alpha_T}{D(\omega'+\omega'')} - \frac{N}{M^3}\frac{\zeta^{(2)}e^{*3}}{D(\omega'+\omega'')D(\omega')D(\omega'')}\right.$$
$$+\frac{N}{M^2}\frac{e^{*2}\gamma^{(2)}}{D(\omega'+\omega'')D(\omega')} + \frac{N}{M^2}\frac{e^{*2}\gamma^{(2)}}{D(\omega'+\omega'')D(\omega'')}$$
$$\left.+\frac{N}{2M}\frac{e^*\alpha_T}{D(\omega')} + \frac{N}{2M}\frac{e^*\alpha_T}{D(\omega'')} + \chi^{(2)}\right). \tag{8}$$

Here the shorthand notation for the denominator factors

$$D(\omega) = \omega_T^2 - \omega^2 - i\omega\Gamma$$

has been introduced. The permutation factor $2-\delta(\omega'-\omega'')$ is 1 for undistinguishable frequencies when $\omega' = \omega''$, and is 2 if the waves are distinguishable.

The first four terms all have resonant denominators at the frequency $\omega'+\omega''$. The terms in $\zeta^{(2)}$ and $\gamma^{(2)}$ can be explicitly dropped and yet their effects implicitly included by a suitable redefinition of α_T. This coefficient will then acquire a weak frequency dependence since ω' and ω'' are far from material resonances. In a similar manner, the effect of other nonresonant terms is taken care of by a redefinition of $\chi^{(2)}$. It can also be shown that all effects of third-order terms in $\zeta^{(3)}$ and $\beta^{(3)}$ can be included in $\chi^{(3)}$. With these constants so redefined, the set of Eqs. (2)–(4) reduces to the following

equivalent set:

$$P_i = Ne^*Q_i + \chi^{(1)}E_i + N\alpha^T_{ijk}E_jQ_k + \chi^{(2)}_{ijk}E_jE_k + \chi^{(3)}_{ijkl}E_jE_kE_l, \tag{9}$$

$$M(\ddot{Q}_i + \Gamma\dot{Q}_i + \omega_T^2 Q_i) = e^*E_i + \tfrac{1}{2}\alpha^T_{ijk}E_jE_k, \tag{10}$$

$$\nabla^2 E_i - [\nabla(\nabla\cdot\vec{E})]_i - \frac{1}{c^2}\frac{\partial^2 E_i}{\partial t^2} = \frac{4\pi}{c^2}\frac{\partial^2 P_i}{\partial t^2}. \tag{11}$$

At this stage Cartesian subscripts have been introduced explicitly for the vector and tensor components. The iteration procedure to third order is still tedious, but straightforward. For two noncollinear beams with arbitrary polarization directions at ω_1 and ω_2, respectively, the result for the three-wave mixing at $\omega_3 = 2\omega_1 - \omega_2$, with an intermediate exciton resonance near $2\omega_1$, is, for the crystal symmetry $\bar{4}3m$, described by

$$\chi^{(3)}_{ijmn,\mathrm{eff}}(-\omega_3,\omega_1,\omega_1,-\omega_2) = \left(\sum_{lp}(A_{inl}A_{pjm}\delta_{lp} - B_{ijl}B_{pmn}\delta_{lp} + B'_{ijl}\times\hat{n}_l\hat{n}_pB'_{pmn} - A'_{inl}\hat{h}_l\hat{h}_pA'_{pjm})\right) + \chi^{(3)}_{ijmn}, \tag{12}$$

where

$$A_{inl}A_{pjm} = U\left(\frac{N\alpha^L_{inl}\alpha^L_{pjm}}{MD_L(2\omega_1)} - \frac{N\alpha^T_{inl}\alpha^T_{pjm}}{2MD_T(2\omega_1)} - \frac{8\pi\chi^{(2)}_{inl}\chi^{(2)}_{pjm}}{\epsilon_\infty}\right) + \frac{N\alpha^T_{inl}\alpha^T_{pjm}}{2MD_T(2\omega_1)}, \tag{12a}$$

$$A'_{inl}A'_{pjm} = (U-1)\left(\frac{N\alpha^L_{inl}\alpha^L_{pjm}}{MD_L(2\omega_1)} - \frac{N\alpha^T_{inl}\alpha^T_{pjm}}{2MD_T(2\omega_1)} - \frac{8\pi\chi^{(2)}_{inl}\chi^{(2)}_{pjm}}{\epsilon_\infty}\right), \tag{12b}$$

$$B_{ijl}B_{pmn} = V(16\pi/\epsilon_\infty)\chi^{(2)}_{ijl}\chi^{(2)}_{pmn}, \tag{12c}$$

$$B'_{ijl}B'_{pmn} = (V-1)(16\pi/\epsilon_\infty)\chi^{(2)}_{ijl}\chi^{(2)}_{pmn}, \tag{12d}$$

$$V = \frac{\epsilon(\omega_1-\omega_2)}{\epsilon(\omega_1-\omega_2) - [\omega_1\epsilon^{1/2}(\omega_1)\hat{m}_1 - \omega_2\epsilon^{1/2}(\omega_2)\hat{m}_2]^2/(\omega_1-\omega_2)^2}, \tag{12e}$$

$$U = \{\epsilon(2\omega_1)/[\epsilon(2\omega_1)-\epsilon(\omega_1)]\}, \tag{12f}$$

$$\alpha^L_{inl} = 2^{-1/2}[\alpha^T_{inl} - (8\pi e^*/\epsilon_\infty)\chi^{(2)}_{inl}], \tag{12g}$$

$$D_L(2\omega_1) = \omega_L^2 - (2\omega_1)^2 - i\Gamma(2\omega_1), \tag{12h}$$

$$D_T(2\omega_1) = \omega_T^2 - (2\omega_1)^2 - i\Gamma(2\omega_1), \tag{12i}$$

where m_i is the unit vector in direction of propagation of beam at ω_i, $\hat{h}_j$ is the jth Cartesian component of $2\hat{m}_1/|2m_1|$, $\hat{n}_j$ is the jth Cartesian component of $(\hat{m}_1-\hat{m}_2)/|m_1-m_2|$, ϵ_0 is the low-frequency dielectric constant, ϵ_∞ is the high-frequency dielectric constant, $\epsilon(\omega)$ is the dielectric constant at frequency ω, and $\omega_L^2 = (\epsilon_0/\epsilon_\infty)\omega_T^2$.

Several assumptions which are valid in the case of CuCl were made in deriving Eq. (12). These are that the crystal is cubic, that the Lyddane-Teller-Sacks relation holds, that light near the exciton energy is highly absorbed, and that Kleinman symmetry can be used. As a result of the $\bar{4}3m$ symmetry of CuCl, only certain components of α^T_{ink}, $\chi^{(2)}_{ijk}$, and $\chi^{(3)}_{ijkl}$ are nonzero. For this symmetry

$$\alpha^T_{ijk} = \alpha^T_{xyz}(1-\delta_{ij})(1-\delta_{ik})(1-\delta_{jk}), \tag{13a}$$

$$\chi^{(2)}_{ijk} = \chi^{(2)}_{xyz}(1-\delta_{ij})(1-\delta_{ij})(1-\delta_{jk}), \tag{13b}$$

and the only nonzero components for $\chi^{(3)}_{ijkl}$ are

$$\begin{aligned} &xxxx = yyyy = zzzz,\\ &yyzz = zzyy = zzxx = xxzz = xxyy = yyxx,\\ &yzyz = zyzy = zxzx = xzxz = xyxy = yxyx,\\ &yzzy = zyyz = zxxz = xzzx = xyyx = yxxy, \end{aligned} \tag{14}$$

where for compactness the indices have been used as labels. Kleinman symmetry results in the further equality

$$yyzz = yzyz = yzzy.$$

In deriving Eq. (12) only the forced excitation at $2\omega_1$ has been kept. The corresponding free-wave solution necessary to match the boundary conditions[22] has been dropped. At the entrance surface of the crystal, both waves have about the same amplitude, proportional to the factor $[\epsilon(2\omega_1)-\epsilon(\omega_1)]^{-1}$. The homogeneous free-wave solution is, however, very heavily damped, as $\epsilon(2\omega_1)$ has a large imaginary part in the frequency range of interest. The

forced excitation at $2\omega_1$ is, of course, present throughout the whole crystal, because the wave at ω_1 propagates without appreciable attenuation, since $\epsilon(\omega_1)$ is real. In second-harmonic generation[14] one measures the effect of this forced wave field at the exit face of the crystal. Only the transverse forced excitation gives rise to a second-harmonic radiation field. In the two-photon and three-wave light-mixing experiments, the longitudinal forced excitation is also observable.

For further discussion it is expedient to consider three simple geometrics, shown in Fig. 2. These take advantage of the $\bar{4}3m$ symmetry properties of the odd-rank tensors α^T_{ijk} and $\chi^{(2)}_{ijk}$ given by Eqs. (13a) and 13(b).

A. No exciton resonance

When the electric fields of the incident waves at ω_1 and ω_2 are parallel to the same cubic axis as shown in Fig. 2(a), no exciton (or phonon) polariton can be excited. There are also no nonresonant electronic polarization and driven electric fields at the intermediate frequencies $2\omega_1$ and $\omega_1 - \omega_2$. In this geometry Eq. (12) reduces to an effective $\chi^{(3)}$ of the form

$$\chi^{(3)}_{\mathrm{NE}} = 2\chi^{(3)}_{xxxx}. \tag{15}$$

The observed three-wave mixing signal is proportional to the square of the real nonresonant susceptibility component $(\chi^{(3)}_{xxxx})^2$. There is no second-harmonic generation and no two-photon absorption in this configuration.

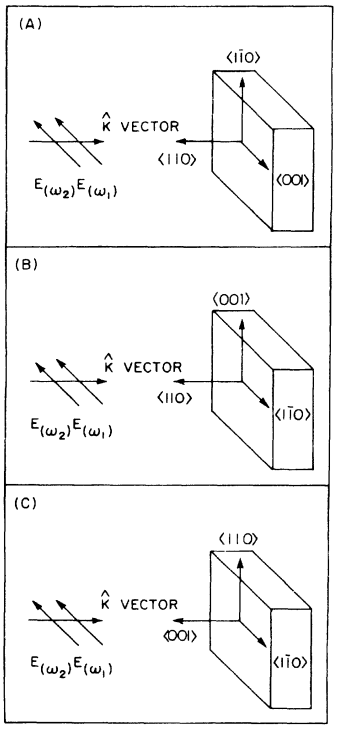

FIG. 2. Relative configuration of the crystal axes and the propagation and polarization directions of the incident laser beams. Three different geometries, discussed as cases in Secs. II A–II C and IV A–IV C, are shown.

B. Transverse polariton excitation

In this configuration both incident waves propagate along the face diagonal [100] and both are polarized with the electric field along [1$\bar{1}$0]. The exciton coordinate and second-harmonic polarization are excited along the cubic z axis [001], according to Eqs. (13a) and (13b), orthogonal to the direction of propagation. The set of Eqs. (12) reduces in this configuration to

$$\chi^{(3)}_{\mathrm{TEP}} = 3\chi^{(3)}_{xxxx} + 9\chi^{(3)}_{xxxx} - V\left(\frac{32\pi}{\epsilon_\infty}\right)(\chi^{(2)}_{xyz})^2 + \frac{1}{\epsilon(2\omega_1) - \epsilon(\omega_1)}\,\frac{1}{D_T(2\omega_1)}\,\frac{2N\alpha^2_{\mathrm{TP}}}{M}, \tag{16}$$

where

$$\alpha^2_{\mathrm{TP}} = \tfrac{1}{2}(\alpha^T_{xyz})^2[\epsilon_\infty - \epsilon(\omega_1)] - 8\pi e^* \alpha^T_{xyz}\chi^{(2)}_{xyz} - D_T(2\omega_1)(M/N)8\pi(\chi^{(2)}_{xyz})^2. \tag{17}$$

The quantity α_{TP} displays a characteristic interference between the nonresonant susceptibility $\chi^{(2)}_{xyz}$ and the excitonic nonlinear coupling coefficient α^T_{xyz}. This type of interference was first observed in difference frequency mixing in infrared phonon-polariton modes by Faust and Henry.[23] The resonance in second-harmonic generation experiments in CuCl, observed by Haueisen and Mahr[14] is related to α^2_{TP}. It may be expected[24] that $e^*\alpha^T_{xyz}$ and $\chi^{(2)}$ have the same sign for $2\omega_1 < \omega_T$, since they both represent the nonlinearity of electronic states in CuCl. Whereas α^T_{xyz} refers specifically to the split-off exciton state, $\chi^{(2)}$ represents a nonlinear property averaged over all the higher electronic bands.[24] At optical frequencies the contribution to $\chi^{(2)}$ from ionic motion is negligible. Thus, at low frequencies, $2\omega_1 < \omega_T$, one may expect reinforcement. Above the transverse exciton frequency $2\omega_1 > \omega_T$, but below the higher electronic resonances so $\chi^{(2)}$ can be considered a constant, the real part of the resonant contribution changes sign with $D_T(2\omega_1)$. Here destructive interference will occur.

Fröhlich *et al.*[16,26] observed this destructive interference in the intensity of two-photon absorption, which is proportional to $\mathrm{IM}\,\chi^{(3)}_{\mathrm{TEP}}$, as given by Eq. (16). Although a resonant denominator $D_T(2\omega)$ appears to multiply the coupling factor α^2_{TP}, one should not expect a resonance to occur for $2\omega_1 = \omega_T$.

The reason is that precisely at this frequency $\epsilon(2\omega_1)$ also goes through resonance. This point has been discussed in detail by several authors.[25] The total response function $\{[\epsilon(2\omega_1)-\epsilon(\omega)]D_T(2\omega_1)\}^{-1}$ is important, and its effect may be summed up in words by saying that a resonance effect may occur only on the undamped polariton dispersion curve, shown in Fig. 1. For two light waves of the same frequency traveling in the same direction, resonance would occur at the point A in Fig. 1. Fröhlich was able to tune along the dispersion curve towards smaller k values by varying the angle between the two light beams. Two-photon absorption occurs at correspondingly lower frequencies. The intensity of the observed signal, proportional to $\mathrm{Im}\,\chi^{(3)}_{\mathrm{TEP}}$ with $\omega_1=\omega_2$, is reproduced in Fig. 3. From this curve it appears that $\alpha_{\mathrm{TP}}=0$ due to destructive interference in Eq. (17) for $2\hbar\omega_1=3.219$ eV. This is accidentally very close for the forward resonant crossing point A, which occurs at $2\hbar\omega_1=3.217$ eV. Fröhlich was not able to observe two-photon absorption if the angle between the incident beams was smaller than 30°.

This has severe implications for the three-wave mixing experiments which give a signal proportional to $|\chi^{(3)}_{\mathrm{TEP}}|^2$. According to Eq. (16) the resonant term must be added to the three nonresonant terms before squaring. For the light waves all traveling in the same forward direction, the resonant term would be very small for the same reason as for collinear two-photon absorption. It could be increased again by taking light waves traveling at a considerable angle, or with widely different frequencies ω_1 and ω_2. Perhaps it should be emphasized again that the observation of a resonance is equivalent to crossing the dispersion curve. Experimentally this is usually done by keeping the direction of the incident light beams fixed and changing the frequency of ω_1. The resonance becomes sharper in frequency for two light beams at ω_1 making a considerable angle with each other. When they travel in opposite directions, one probes the exciton polariton at $\vec{k}=0$. In this case, the transverse and longitudinal excitations are degenerate and undistinguishable.

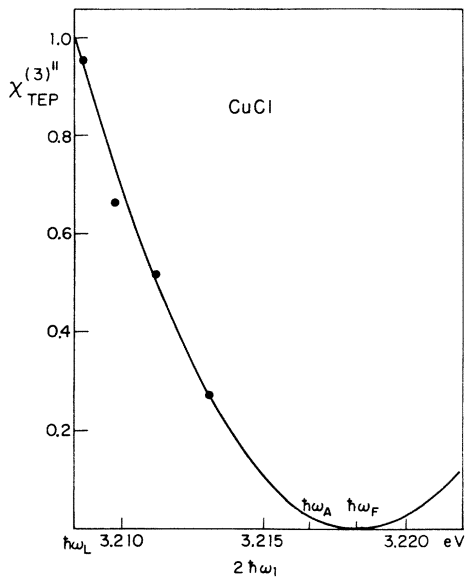

FIG. 3. Integrated two-photon absorption coefficient as a function of the transverse exciton-polariton frequency. The vertical scale is normalized to unity for the imaginary part of $\chi^{(3)}_{\mathrm{TEP}}$ of Eq. (16) for $2\omega_1=\omega_L$ [after Fröhlich (Ref. 16)].

C. Longitudinal exciton configuration

In the geometry of Fig. 2(c), the light beams propagate along the cubic axis [001], while their electric fields remain parallel to the $[\bar{1}10]$ face diagonal. This geometry differs only from the transverse configuration by turning the crystal 90° around the $[\bar{1}10]$ direction. The second-harmonic polarization and exciton coordinate are again parallel to [001], which is now also the direction of the wave vector $2\vec{k}_1$. For this configuration the set of Eqs. (12) reduces to

$$\chi^{(3)}_{\mathrm{LE}}=\left(3\chi^{(3)}_{xxxx}+9\chi^{(3)}_{xyxy}-\frac{32\pi(\chi^{(2)}_{xyz})^2}{\epsilon_\infty}\right)+\frac{2N\alpha^{L^2}_{xyz}}{MD_L(2\omega_1)} \tag{18}$$

with

$$2(\alpha^L_{xyz})^2=\left(\alpha^T_{xyz}-\frac{8\pi e^*}{\epsilon_\infty}\chi^{(2)}_{xyz}\right)^2. \tag{19}$$

Equation (18) shows, as expected, a resonant behavior for $2\omega_1=\omega_L$, where the longitudinal polariton dispersion curve is crossed. As remarked earlier, ω_L is a constant for the wave vectors of interest. At the resonant frequency, $2\omega_1=\omega_L>\omega_T$, there is again a destructive interference in the nonlinear coupling coefficient, as given by Eq. (19).

In this configuration no second-harmonic generation of radiation can be detected in transmission because of the longitudinal character of the polarization. Two-photon absorption has, however, been observed by Fröhlich *et al.*[26] in a signal proportional to $\mathrm{Im}\chi^{(3)}_{\mathrm{LE}}$, with $\omega_1=\omega_2$. The three-wave light-mixing signal at $2\omega_1-\omega_2$ has an intensity proportional to $|\chi^{(3)}_{\mathrm{LE}}|^2$. This signal exhibits an interference between the real part of the resonant term and the three nonresonant bracketed terms occurring in Eq. (18). As $\hbar\omega_L=3.208$ eV is now farther removed from $\hbar\omega_F=3.219$ eV where cancellation of the nonlinear coupling occurs, and as the horizontal longitudinal dispersion curve is crossed at nearly right angles for a variation of the frequency ω_1, the opportunity to observe a

sharp resonance is much better in this longitudinal geometry.

D. Theory of double resonance

So far only the resonant contribution of the Z_3 exciton has been considered. Other excitations may be considered, separately or simultaneously, by introducing more than one variable Q. In three-wave light-mixing experiments creating an output intensity at $2\omega_1 - \omega_2$, intermediate resonances at $2\omega_1$ and $\omega_1 - \omega_2$ are important, as was already mentioned in the Introduction.[2] In CuCl, in particular, interesting double-resonance-interference effects may be expected if $2\omega_1$ is near the Z_3-exciton resonance, while simultaneously $\omega_1 - \omega_2$ is close to the longitudinal, optical phonon-polariton infrared frequency at ω_R. The symmetry properties of the coupling parameters of the phonon polariton are similar to those for the exciton. The three geometries of Fig. 2 also refer to the cases of no resonance, transverse and longitudinal excitation for the phonon polariton. A resonance can now occur at an intersection of the difference frequency dispersion curve with a branch of the undamped phonon polariton curve.

This can be treated theoretically by introducing two normal coordinates Q_E and Q_R for the exciton and phonon polariton, respectively. Add the subscript E to all quantities referring to the exciton to distinguish them from the corresponding quantities for the phonon polariton which are labeled by R. The phonon polariton can be excited by a Raman-type two-photon process. The reduced mass of the phonon polariton is M_R. The longitudinal phonon-polariton frequency is ω_{LR}. The nonlinear coupling coefficient to it is denoted by $\alpha^{\mathrm{LR}}_{xyz}$, given by an expression analogous to Eq. (19) or (12g). All preceding arguments may be repeated. Detailed microscopic considerations and complete calculations of Flytzanis[4] show that the effects of the two resonances are additive. The longitudinal configuration is most important for the double-resonance-interference phenomena from an experimental point of view. The observed intensity at $2\omega_1 - \omega_2$ is proportional to $|\chi^{(3)}_{\mathrm{LDR}}|^2$ in this case, which is a straightforward extension of Eqs. (18) and (19)

$$\chi^{(3)}_{\mathrm{LDR}} = 3\chi^{(3)}_{xxxx} + 9\chi^{(3)}_{xyxy} - \frac{32\pi(\chi^{(2)}_{xyz})^2}{\epsilon_\infty} + \frac{2N_E(\alpha^{\mathrm{LE}}_{xyz})^2}{M_E D_{\mathrm{LE}}(2\omega_1)} + \frac{4N_R(\alpha^{\mathrm{LR}}_{xyz})^2}{M_R D_{\mathrm{LR}}(\omega_1 - \omega_2)}. \tag{20}$$

The resonant frequency of the longitudinal optical phonon mode in CuCl occurs at 0.026 eV at 16 °K. The Raman term contains an extra factor of 2, because of the possible permutation of the frequencies ω_1 and $-\omega_2$. A detailed discussion of these nonlinear dispersive characteristics will be postponed to Sec. IV.

E. Local-field corrections

Thus far the fields acting on the electrons have been put equal to the macroscopic fields occurring in Maxwell's equations. For extended orbitals, which probe essentially the spatially averaged microscopic fields, this is a good first approximation. For localized orbitals centered at a point of cubic symmetry, Lorentz-Lorenz-type correction factors must be applied. For direct nonlinear processes in cubic crystals these are well known,[6]

$$\chi^{(2)}_{(-2\omega_1,\omega_1,\omega_1)} = \chi^{(2)}_c(-2\omega_1,\omega_1,\omega_1) \times\left|\tfrac{1}{3}[(3-A)+A\epsilon(2\omega_1)]\,\tfrac{1}{3}[(\epsilon-A)+A\epsilon(\omega_1)]^2\right|, \tag{21}$$

$$\chi^{(3)}_{(-\omega_3,\omega_1,\omega_1,-\omega_2)} = \chi^{(3)}_c(-\omega_3,\omega_1,\omega_1,-\omega_2) \times\left|\tfrac{1}{3}[(3-A)+A\epsilon(\omega_3)]\,\tfrac{1}{3}[(3-A)+A\epsilon(\omega_1)]^2 \times\tfrac{1}{3}[(3-A)+A\epsilon(\omega_2)]\right|, \tag{22}$$

where $\chi^{(2)}$ and $\chi^{(3)}$ are the nonlinearities actually measured experimentally and $\chi^{(2)}_c$ and $\chi^{(3)}_c$ would be the susceptibilities found if there were no local-field corrections. A, which ranges from 0 to 1, is a measure of the localization of the electron eigenstates in real space and so is a parameter that determines the importance of the effect. $A = 1$ corresponds to localized point wave functions and so to a maximum local-field correction. In contrast, $A = 0$ means the wave functions are smeared out over the unit cell and so no local-field effects occur.

Since the crystal is transparent at ω_1, ω_2, and ω_3, $\epsilon(\omega_1)$, $\epsilon(\omega_2)$, and $\epsilon(\omega_3)$ are real constants and the local-field correction only changes the value of $\chi^{(3)}_c$ to another real constant. However, $\epsilon(2\omega_1)$ has considerable frequency dispersion for $2\omega_1 \approx \omega_T$ and so if local-field effects are important, $\chi^{(2)}$ also will have a dramatic frequency dependence. $\chi^{(2)}$ has already been measured in a second-harmonic generation experiment.[27] In this experiment both the fundamental and second-harmonic waves were in the transparent region of CuCl. This energy regime was chosen since it allows the most accurate determination of $\chi^{(2)}$.

Since a real electric field is generated at the intermediate frequency $2\omega_1$ in the two-step process

but not in the direct process, it is reasonable to expect an additional local-field correction for the former process. This, in fact, has been shown to be true,[28] and it was found that the longitudinal polariton response function $1/\epsilon(2\omega_1)$ should actually be replaced by $[1/\epsilon(2\omega_1)]\{(3-A)/[(3-A)+A\epsilon(2\omega_1)]\}$. So including local-field corrections to both direct and indirect processes means that $(\chi^{(2)}_{xyz})^2$ should be replaced by $[F(A)](\chi^{(2)}_S)^2$, where

$$F(A)=\frac{(3-A)[(3-A)+A\epsilon(2\omega_1)]}{[(3-A)+A\epsilon_0]^2} \tag{23}$$

and $\chi^{(2)}_S$ is the value for the second-order optical susceptibility found in the second-harmonic experiment. The function $F(A)$ varies rapidly only in the immediate vicinity of ω_T when $3.195 \lesssim 2\hbar\omega_1 \lesssim 3.205$ eV. This is many exciton linewidths away from the longitudinal exciton energy, $2\hbar\omega_1 = \hbar\omega_L \approx 3.208$ eV. The local-field effect would therefore appear mainly as a modulation in the third-order susceptibility below the exciton resonance. A departure from a simple Lorentzian near the exciton peak due to the change in the real part of $F(A)$ near $2\omega_1 \sim \omega_L$ might also be noticeable. However, as seen from the experimental results that will be presented in Sec. IV, no such effects were apparent, and so for this experiment at least the local-field effects in CuCl do not lead to an additional frequency dependence.

III. EXPERIMENTAL APPARATUS

The basic requirement of nonlinear optical spectroscopy is a high-powered tunable laser with an output in the proper region of the spectrum. For the experiment described in this paper, this necessity was met by the use of a ruby laser pumped tunable dye laser.[18] The dye laser output wavelengths required for this study are determined by the conditions that $\hbar\omega_1 + \hbar\omega_2 \approx \hbar\omega_L$ and $\hbar\omega_1 - \hbar\omega_2 \approx \hbar\omega_R$ where $\hbar$ in Planck's constant. ω_1 and ω_2 are the dye laser angular frequencies, while $\hbar\omega_L$ is the energy of the longitudinal CuCl Z_3 exciton and $\hbar\omega_R$ is the energy of the longitudinal optical Raman mode. From linear measurements $\hbar\omega_L \approx 3.208$ eV and $\hbar\omega_R \approx 0.026$ eV at liquid-helium temperatures[13,29] and so the required laser wavelengths are $\lambda_1 = 2\pi c/\omega_1 \approx 7700$ Å and $\lambda_2 = 2\pi c/\omega_2 \approx 7825$ Å, where c is the speed of light. To be able to follow temperature shifts of the exciton and to scan across the full structure of the resonance, the lasers should also be independently tunable over the range from about 7600 to 8000 Å.

Fortunately, several reasonably efficient dyes are known to function in this region.[30-32] In particular, two polymethine dyes 3, 3′-dimethyl-2, 2′-oxatricarbocyanine iodide (DMOTC iodide) and 1, 3, 3, 1′, 3′, 3′-hexamethyl-2, 2′-indotricarbocyanine iodide (HMITC iodide) purchased from Nippon Kankoh-Shikiso and Eastman Kodak Chemical, respectively, were used. Certified grade dimethyl sulfoxide (DMSO) supplied by Fisher Scientific was chosen as the solvent since it is known to be almost without exception the most efficient vehicle for polymethine dyes.[33,34] The optimum dye concentration varied with wavelength, but a mixture of 6×10^{-5}-mole/l DMOTC iodide with 0.2×10^{-5} mole/l of HMITC iodide was found to be suitable over most of the energy range studied.

The ruby laser used was a modified Raytheon model SS-420. It was capable of producing a stable, actively Q switched, polarized, multimode, 20-MW pulse at a repetition rate of one shot per second. This relatively high, for a ruby laser, pulse rate greatly simplified both the alignment of the experimental optical train and the actual taking of data.

The experimental apparatus used for studying the interference in $\chi^{(3)}$ due to simultaneous intermediate frequency excitation of a Raman and exciton mode is shown in Fig. 4. The ruby laser beam was physically split so that it pumped two separate regions of the flowing dye cell. One portion of the cell served as the active region of the dye laser that produced the beam at ω_1. The other pumped region was the active element for a second dye laser which served as the source of photons at frequency ω_2. Since two photons at frequency ω_1 are needed for every photon at frequency ω_2, the dye laser at ω_1 was adjusted to have twice the energy per pulse as the dye laser at ω_2 in order to optimize the generation efficiency of the signal at $2\omega_1 - \omega_2$.

The cell which contained the dye solution consisted of a 304 stainless-steel housing 2 cm long with uncoated fused silica windows. The windows were

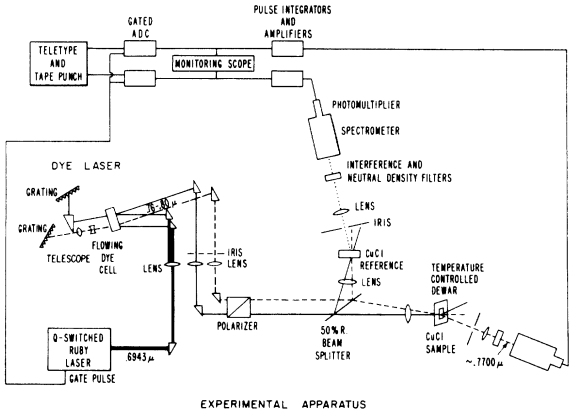

FIG. 4. Schematic of experimental apparatus for the generation of light at $2\omega_1 - \omega_2$ by two tunable incident dye laser beams at ω_1 and ω_2, respectively.

wedged at an angle of 5° with respect to each other in order to prevent intracell feedback. As a result of the high gain of the dye laser, the uncoated exit window of the dye cell was able to serve as the output mirror. The normal to this window which was used to define the dye laser axis was at an angle of about 2° with respect to the ruby pump beams. This allowed the cell to be essentially longitudinally pumped and still have spatial separation of the dye and ruby rays.

The rear cavity reflectors for both dye lasers were gold coated, 1200 lines/mm Bausch and Lomb No. 35-53-08-530 plane gratings which were blazed for 1 μm. These gratings, which were used in second order in a Littrow configuration, served as the frequency dispersive elements in the cavities. The gratings were held in two separate Lansing mounts equipped with differential micrometer screws and could be tuned independently.

An inverted 10X telescope (Oriel B34-60) was placed between the dye cell and the grating in the dye laser cavity which generated the ω_1 photons for the purposes of beam expansion and collimation. This ensured that the light striking the dispersive element was made up of parallel rays and that the beam illuminated a large enough number of grooves for good resolution.

The actual outputs of the dye lasers were found to be multimode pulses with a 15-nsec full width at half-maximum length and a maximum total energy of about 0.008 J/pulse. This gave a 0.5-MW pulse with about a 5% power-conversion efficiency. The linewidth of the ω_1 laser was measured with an air-spaced Fabry-Perot etalon to be about 0.1 Å, corresponding to an energy resolution in $2\hbar\omega_1$ of 4×10^{-5} eV ≈ 0.3 cm^{-1} which was fine enough to resolve the exciton peak. The linewidth of the ω_2 laser was several times larger than this, since this laser did not contain an intracavity beam expender. Dye laser output wavelength versus micrometer screw setting at various wavelengths in the region of interest was found photographically using Polaroid 413 infrared film (no longer manufactured), a krypton calibration lamp and a Spex model 1700-111 $\frac{3}{4}$-m Czerny-Turner spectrometer. This gave an absolute wavelength calibration correct to 0.3 Å with a negligible error in reproducibility.

As shown in Fig. 4, the output of the dye lasers at frequencies ω_1 and ω_2 first passed through irises placed about 50 cm from the output window. This served to block most of the spontaneous fluorescence. They then passed through 100-cm-focal-length lenses, which served to reduce the beam divergence. A single air-spaced Glan laser polarizer, which had a rejection ratio of 10^{-4} was placed in the optical train to ensure that both beams were polarized in the same direction. The rays were then focused and overlapped inside a CuCl sample crystal, which was placed in a variable-temperature helium cryostat, and a CuCl reference crystal by means of separate 20-cm-focal-length room-temperature lenses and a 50/50 beam splitter. Any substantially tighter focusing damaged the CuCl crystals. The CuCl reference crystal was oriented in the configuration where symmetry dictated no dispersion in $\chi^{(3)}$. Also, since it was at room temperature, the exciton and Raman modes were heavily damped anyway.

For a cubic crystal, using the material under study as its own reference greatly simplifies the phase-matching requirements of the experiment, since the same angle between the incident beams can be used in both arms of the apparatus. However, in order for this procedure to be valid, it must be shown that there is an orientation where $\chi^{(3)}$ is independent of frequency. A preliminary set of experiments in which the three-wave mixing signal in CuCl was compared to that from a primary reference crystal of NaCl, which was known to be dispersionless in the frequency range studied, demonstrated that this was indeed true for CuCl, as will be shown in Sec. IV A. In this initial experiment only one dye laser was used, and a portion of the ruby beam itself contributed the photons at ω_2. An additional set of prisms in the sample arm compensated for the difference in phase match matching angles in the two materials.

The output signal as a result of the nonzero phase-matching angle was produced at an angle of about 1° from the incident beams, and therefore small irises placed about 10 cm from the crystals could be used to block the incident photons from the rest of the optical train. A 5-cm-focal-length lens focused the output signal, which passed through the iris through interference filters onto the entrance slit of a spectrometer. A $\frac{1}{4}$-m Jerral-Ash was used in the sample arm, and a $\frac{1}{2}$-m Spex was used in the reference arm. Calibrated neutral-density filters could also be inserted at this point to prevent the detection photomultiplier from saturating. While the spectrometers were useful in determining the output frequency and thus served to check that the proper three-wave mixing signal was actually being observed, their additional wavelength rejection was not absolutely necessary. In fact, during an experimental run the spectrometer gratings were replaced by mirrors. This eliminated the need to tune the spectrometers as the output wavelength changed during the course of the experiment.

The signal photons were detected by a low-noise RCA C31025J photomultiplier which had a quantum efficiency of about 10% at the output wavelength

near 7600 Å. The electrical pulse from the photomultiplier was integrated, amplified, and digitized using standard electronic techniques. An oscilloscope was used to monitor the amplifier output in order to check for signal saturation. A number which was directly related to the number of signal photons from each crystal was then printed on an ASR33 teletype and tape punch. The tape, which had information on amplifier gain, filter factors, and wavelength entered manually on it, was then read and analyzed on a Hewlett-Packard 9820A programmable calculator using a special data-reduction program written for this experiment.

Before starting any run, three checks were made to ensure that the output signal was indeed due to the three-wave mixing process of interest. First the spectrometer was used to make sure that the output signal at ω_3 had the proper frequency. Second, the ω_1 beam was blocked. Since a signal at $2\omega_1 - \omega_2$ requires a beam at ω_1, blocking the ω_1 beam should eliminate the output signal. In general a small signal due to fluorescence in the dye cell and scattering in the crystal remained. A similar test, with only the ω_2 beam blocked, was also made. The amount of electrical noise was checked by blocking both beams. Noise due to spurious light, dark current, electrical pickup, and all other sources could always be adjusted to be less than 1% of the lowest-level three-wave mixing signal measured during any experimental run.

The basic experimental procedure for the study of the exciton resonance contribution to the mixing nonlinearity $\chi^{(3)}(-2\omega_1+\omega_2, \omega_1, \omega_1, -\omega_2)$ was to measure the intensity $I(2\omega_1 - \omega_2)$, with ω_2 kept constant, while $2\omega_1$ was varied through the frequency range containing the exciton resonances. A plot of the average ratio of the CuCl signal, at each frequency, to the signal from the reference crystal would then give the dispersive behavior of $|\chi^{(3)}|^2$. In the double-resonance experiments, $2\omega_1$ was kept constant in the vicinity of the exciton resonance, while ω_2 was varied so that $\omega_1 - \omega_2$ was swept through the infrared phonon-polariton resonance. The procedure was then repeated for several values of $2\omega_1$ near the exciton resonance peak.

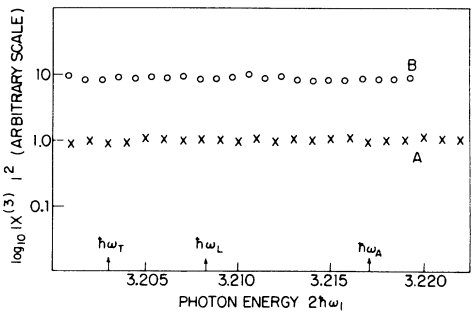

FIG. 5. Three-wave mixing signal $I(2\omega_1 - \omega_2)$, as $2\omega_1$ is varied across the region containing the frequencies ω_T, ω_L and ω_A indicated in Fig. 1. The experimental points × refer to the no-exciton configuration of Fig. 2(a). The experimental points ○ refer to the transverse exciton configuration of Fig. 2(b).

This basic plan, however, was modified somewhat to eliminate intrinsic frequency response of the experimental system which was still present due to the inequality in the two arms of the comparison system. A frequency run was always made with both CuCl crystals in the no excitation configuration. The frequency trends still occurring due to system spectral response could thus be measured and the data in the sample run corrected correspondingly.

IV. EXPERIMENTAL RESULTS OF THREE-WAVE MIXING IN CuCl

These results will be presented in the same order as the theoretical treatment in Sec. II to facilitate the discussion and theoretical interpretation.

A. No exciton configuration

In the geometry of Fig. 2(a), with all electric field vectors parallel to one cubic axis, no resonances are expected. The observed intensity $I(2\omega_1 - \omega_2)$ in CuCl at 15.4 °K is presented by crosses in Fig. 5 as a function of $2\omega_1$. There is no evidence of any variation with frequency, as expected from the theory, which shows that the intensity should be proportional to $|3\chi^{(3)}_{xxxx}|^2$. In order to calibrate this quantity, a comparison experiment was made for three-wave mixing in diamond. A diamond, for which the third-order mixing susceptibility had been measured previously, albeit at shorter wavelengths, replaced the CuCl inside the cryostat at room temperature. For this comparison it is necessary to know the effective phase-matching length $\sin(\frac{1}{2}\Delta kL)/(\frac{1}{2}\Delta k)$ in each sample where Δk is the three-wave mixing phase mismatch and L is the sample length. This function was determined by a variation of the angle between the two light beams in each crystal, which were about 1 mm thick. The intensity was observed to follow the theoretical pattern $\sin^2(\frac{1}{2}\Delta kL)/(\frac{1}{2}\Delta k)^2$. For $\Delta kL \ll 1$, which was the condition in this experiment, the correction factor to be applied consists of the ratio of the square of the thickness of the two crystals and the ratio of some Fresnel factors for transmission of light. The data of Levenson and Bloembergen[2] for diamond taken for $4.4 < 2\hbar\omega_1 < 6.2$ eV were extrapolated to $2\hbar\omega_1 \sim 3.1$ eV by means of the frequency dependence discussed by these authors. $\chi^{(3)}_{xxxx}$ in diamond is proportional to $(W_-$

$-\hbar\omega_1)^{-2}(W_+ - 2\hbar\omega_1)^{-1}$, where $W_- \sim 7$ eV is somewhat above the indirect band gap and $W_+ \sim 12.5$ eV, which corresponds to the average energy of electronic states in the conduction band with the same parity as the valence band. This extrapolation leads to the value $\chi^{(3)}_{xxxx}$ (diamond, $2\hbar\omega_1 \sim 3.22$ eV) $= (2.8 \pm 0.5) \times 10^{-14}$ cm^3/erg. Experimentally $|3\chi^{(3)}_{xxxx} + i\chi''^{NR}_{xxxx}|$ was found to be 15 times larger. Here allowance has been made for the existence of a background two-photon absorption process. This leads to a nonresonant imaginary contribution to the third-order susceptibility. Unfortunately, this quantity is not known independently. All that can be concluded at this stage is that $|\chi^{(3)}_{xxxx}(\text{CuCl})| < 14 \times 10^{-14}$ cm^3/erg.

B. Transverse exciton configuration

The data for this case are shown as open circles in Figure 5. It is seen that the nonresonant intensity is a factor ten times larger than in case A. According to Eqs. (15) and (16) one finds,

$$|3\chi^{(3)}_{xxxx} + 9\chi^{(3)}_{xyxy} - V(32\pi/\epsilon_\infty)(\chi^{(2)}_{xyz})^2| = 13.4 \times 10^{-13} \text{ cm}^3/\text{erg}.$$

For this geometry $V \sim -5$, as determined by Eq. (12e). The value of $\chi^{(2)} = -6(\pm 3) \times 10^{-8}$ (cm^3/erg)$^{1/2}$ follows from earlier work.[27] Thus, $-V(32\pi/\epsilon_\infty)(\chi^{(2)})^2 \sim 5 \times 10^{-13}$ cm^3/erg, and $\chi^{(3)}_{xxxx} + 3\chi^{(3)}_{xyxy} \sim 3 \times 10^{-13}$ cm^3/erg.

There is no indication in the experimental data of the resonance term in Eq. (16), proportional to α^2_{TP}. This disappointing result is due to the near cancellation of the contributions in Eq. (17). The transverse polariton resonance would be expected to occur at $2\hbar\omega_1 = \hbar\omega_A = 3.217$ eV, where according to Fig. 3, $\alpha_{TP} \approx 0.07\alpha^T_{xyz}$. Exact cancellation with $\alpha_{TP} \sim 0$ occurs for $2\hbar\omega_1 \approx 3.219$ eV. It is estimated that the ratio of the resonant to the nonresonant contribution has a maximum of less than 0.2, and so no observable resonance effect could be expected. This is in marked contrast to the pronounced resonance which occurs in the longitudinal configuration. One might expect the transverse exciton resonance to be observable in other crystals. The near cancellation of the terms in α_{TP} at the intersection point A for forward matching is probably an unfortunate accidental characteristic of CuCl. It is very difficult in the three-wave mixing experiment to permit a large angle between two different beams at ω_1, as was done in the two-photon absorption experiments, and such experiments were not attempted.

C. Longitudinal exciton configuration

Much more information and spectroscopic nonlinear data are obtainable from three-wave mixing experiments in the geometry of Fig. 2(c) in which a resonance was actually observed. The intensity $I(2\omega_1 - \omega_2)$ for CuCl at 14.9 °K in this longitudinal orientation is shown in Fig. 6 as a function of $2\hbar\omega_1$. This intensity should be proportional to $|\chi^{(3)}_{LE}|^2$ as given by Eq. (18). The drawn curve A, calculated from this equation, fits the maximum near $2\omega_1 = \omega_L$ very well, but the minimum is much less pronounced in the experimental data which is denoted by the crosses. This dip below the baseline results from a near cancellation of the nonresonant part and the real part of the resonant term above the resonant frequency. The strength of the minimum is determined by the magnitude of the imaginary part of $\chi^{(3)}_{LE}$. A small imaginary part will result in a sharp dip. Filling in of the minimum has been attributed in other cases to a background two-photon absorption process.[2] Unfortunately, direct two-photon absorption studies are not sensitive enough to measure this effect directly in CuCl.[26,35] However, we are inclined to invoke the same explanation, because we have *verified* that the background due to scattering and loss of polarization definition in our strained CuCl crystals was smaller than the minimum signal in the curve. If a term $i\chi''^{(3)}_{NR}$ is added to Eq. (18) to account for this absorption, a very good fit with the experimental data can be obtained. This is indicated by curve B in Fig. 6, where

$$\chi''_{NR} = 0.5\chi'_{NR} = 0.5[3\chi^{(3)}_{xxxx} + 9\chi^{(3)}_{xyxy} - 32\pi\epsilon_\infty^{-1}(\chi^{(2)}_{xyz})^2].$$

The fit to the experimental data yields the values for the resonant frequency, the damping parameter, and the nonlinear coupling coefficient of the longi-

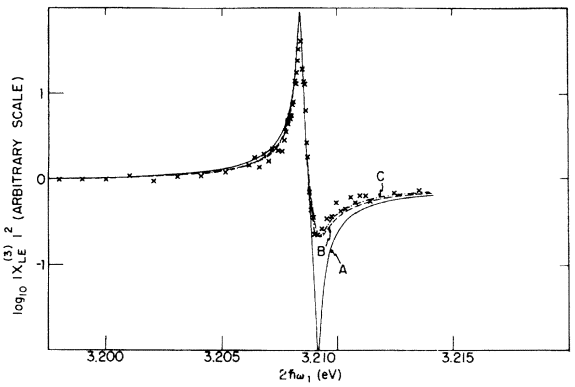

FIG. 6. Three-wave mixing signal $I(2\omega_1 - \omega_2)$, as $2\omega_1$ is varied across the longitudinal Z_2 exciton. Experimental points are indicated by ×. Curve A: Theoretical fit without corrections. Curve B: Theoretical fit with a correction for background two-photon absorption. Curve C: Theoretical fit with an assumed correction for scattering by strain-induced birefringence. To obtain this fit, a scattering many times larger than the experimentally observed scattering had to be assumed.

tudinal exciton. Our results are $\hbar\omega_L = 3.2083 \pm 0.0002$ eV, $\hbar\Gamma_L = (1.5 \pm 0.4) \times 10^{-4}$ eV, and $|2N(\alpha^L_{xyz})^2\hbar^2/M\chi'_{NR}| = 0.005 \pm 0.001$ eV^2. The longitudinal exciton energy $\hbar\omega_L$ agrees within the experimental error to that found in two-photon absorption studies.[16,26,35] Since the instrumental linewidth was found in Sec. III to be less than 0.4×10^{-4} eV, the measured value of the damping constant $\hbar\Gamma_L$ is very close to the actual value. This value for $\hbar\Gamma_L$ agrees well with an estimate from two-photon absorption measurements[26] of 1.2×10^{-4} eV.

The nonresonant signal was again compared with the signal in diamond by the same procedure described for the no exciton geometry. It was found that the longitudinal nonresonant signal was about one-fourth the value for the transverse configuration. This is due to the different nonresonant parts in Eqs. (16) and (18). Since the longitudinal configuration does not contain the term V which is only approximately known, it yields the best determination for $\chi^{(3)}_{xxxx} + 3\chi^{(3)}_{xyxy} = (2.8 \pm 1.8) \times 10^{-13}$ cm^3/erg. From a comparison with data reported at the beginning of this section, one may conclude that χ_{xyxy} has the same order of magnitude as $\chi^{(3)}_{xxxx}$. Nor more precise conclusions can be drawn because of the uncertainty in the nonresonant two-photon background, which may have its own unknown anisotropy.

A measure of the strength of the resonance is given by the quantity α_L^2 given by Eq. (12g). For $2\omega_1 = \omega_L$ there is still destructive interference embodied in the last factor on the right of Eq. (12g), but the cancellation is not nearly as complete as that found in the transverse case. One finds $8\pi e^* \chi^{(2)}_{xyz}/\epsilon_\infty \alpha^T_{xyz} \sim 0.3$, where the value of $\alpha^T_{xyz} = (3.9 \pm 2.2) \times 10^{-17}$ cm^2 obtained from two-photon absorption data[16,24,26] is used, while $\chi^{(2)}$ is again known from data on second-harmonic generation.[27]

With the values for the reduced mass of $M = 0.406$ times the electron mass and $N = 3.8 \times 10^{21}$ cm^{-3} for the density of chlorine atoms, the curve fitting with the experimental data in Fig. 6, in conjunction with the three-wave mixing calibration in diamond, yields the experimental result $|\alpha^L_{xyz}| = (2.1 \pm 1.3) \times 10^{-17}$ cm^2. When the positive value for α^L is chosen and inserted in Eq. (12g), one finds $\alpha^T_{xyz} = (4.2 \pm 3.0) \times 10^{-17}$ cm^2. This agrees well with the value determined from Fröhlich's two-photon absorption data. The negative value of α^L_{xyz} would lead to a negative value of α^T_{xyz}. This would be inconsistent with the experimental data of Haueisen,[16] which require $\alpha^T_{xyz} > 0$, to explain the observed frequency dependence for second-harmonic generation. This argument makes use of a negative experimental value[27] $\chi^{(2)}_{xyz} = -6(\pm 3) \times 10^{-8}$ (cm^3/erg)$^{1/2}$. Earlier use of this same argument[6] had led to the erroneous statement that α^T_{xyz} was negative, because of the wrong choice of sign of e^*.

The magnitude of α^L(or α^T) could also be derived from the intensity of second-harmonic generation, or from a direct absolute determination of the two-photon absorption cross section. Both these methods are inaccurate. The first because it requires detailed knowledge of the dielectric constant in a highly absorbing region and the second because it is very difficult to obtain an accurate determination of the spatial distribution of the intensity in the beam. The intensity dependent absorption coefficients reported by Fröhlich *et al.*[26] and Bivas *et al.*[35] would correspond to a value of the imaginary part of the nonlinear susceptibility which is an order of magnitude smaller than our observed value at the longitudinal exciton resonance at 14.9 °K, which was

$$\chi''_{LE}(\omega_1, \omega_2, -\omega_2) = 4N\hbar^2(\alpha^L_{xyz})^2/M\hbar\omega_L\hbar\Gamma = (1.6 \pm 1.2) \times 10^{-11} \text{ cm}^3/\text{erg}.$$

This corresponds to a two-photon absorption coefficient of 0.9 ± 0.6 cm^{-1} at an intensity of 20 MW/cm^2. The second-harmonic data of Haueisen and Mahr[14] led to a value α^T_{xyz}, which is a factor of 2 larger than those found by either three-wave mixing or from the dispersion of the intensity of two-photon absorption shown in Fig. 3. These latter two methods perform an intrinsic calibration by interference effects in the nonlinear coupling coefficient. In Fröhlich's two-photon absorption data of Fig. 3, α^T_{xyz} is compared with $\chi^{(2)}_{xyz}$, while in the three-wave mixing experiments $(\alpha^L_{xyz})^2$ is compared with nonresonant contribution to $\chi^{(3)}$. These methods are inherently more accurate.

1. Temperature dependence of longitudinal exciton resonance

The three-wave mixing method has been used to study the temperature dependence of the resonant frequency and the damping of the longitudinal exciton. The temperature dependence of the observed

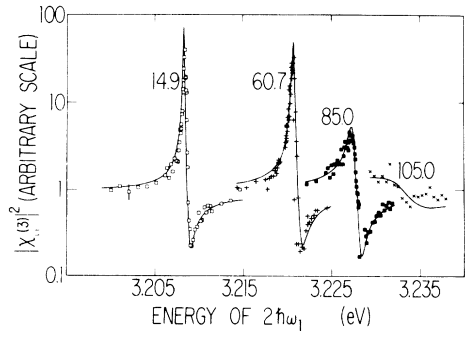

FIG. 7. Temperature dependence of the dispersion in $|\chi^{(3)}_{LE}|^2$ near the Z_3 longitudinal exciton in CuCl. The numbers labeling the curves are °K.

resonance in $|\chi^{(3)}_{LE}|^2$ is shown in Fig. 7. The solid lines are curves fit to Eq. (18) with a nonresonant imaginary part added. Data at 15 different temperatures in the range from 5 to 105 °K were taken, although Fig. 7, for clarity, includes only those curves measured at 14.9, 60.7, 85.0, and 105.0 °K. Above 105 °K the resonance peak could no longer be seen, although photoconductivity studies[36,37] seem to indicate that direct thermal quenching of the longitudinal exciton begins to occur at about 150 °K. In the temperature range covered the ratio of the nonresonant part of $\chi^{(3)}$ to $(\alpha_L)^2$ is a constant. The changes in line position and shape can be accounted for completely by the variation with temperature of $\hbar\omega_L$ and $\hbar\Gamma_L$ which are plotted in Figs. 8 and 9, respectively.

The solid line in Fig. 8 is a least-squares fit to the data points that lie above 30 °K. Above this temperature, the longitudinal exciton energy is linearly dependent on temperature with a slope of 2.9×10^{-4} eV/°K. This value is in close agreement with that found from luminescence experiments.[13,38] As Cardona[13] points out, the sign and magnitude of the slope is due to a competition between the electron-phonon interaction (explicit temperature effect) and the temperature dependence of the lattice constant (volume effect).

The logarithm of the damping constant $\hbar\Gamma_L$ is plotted as a function of temperature in Fig. 9. The temperature dependence of $\hbar\Gamma_L$ can be fitted by the sum of a constant impurity- or strain-dominated part and an exponential term, which is indicative of a multiphonon process. This behavior is shown by the solid line in Fig. 9. A temperature variation of this type suggests that the Z_3 exciton can make a transition to the nearest diffuse $Z_{1,2}$-exciton level. These two levels are separated by an almost-temperature-independent constant of 0.07 eV.[37] This transition would require the simultaneous absorption of three longitudinal optical phonons which couple strongly to the heavy Z_3-exciton state.[8,9] The longitudinal optical phonons

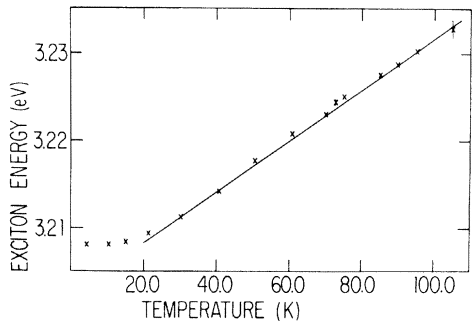

FIG. 8. Temperature dependence of the resonant frequency ω_L of the Z_3 longitudinal exciton in CuCl.

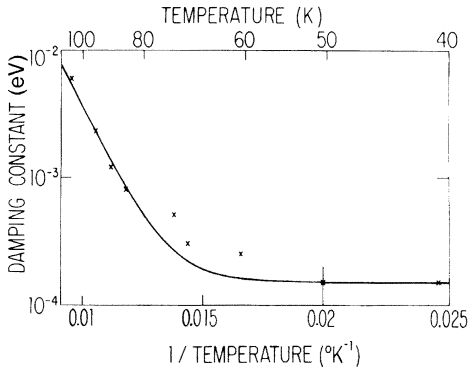

FIG. 9. Temperature dependence of the width $\hbar\Gamma_L$ of the Z_3 longitudinal exciton in CuCl.

have an energy of about 0.025 eV each, so that a small energy balance may have to be taken up by acoustic phonons. The required change in spin configuration can be supplied by the large spin-orbit interaction. In this case, the theoretical temperature dependence would be given by

$$\Gamma = \Gamma_0 + \overline{B}|1/(e^{\hbar\omega_R/KT} - 1)|^3, \tag{24}$$

where the second term is cubic in the phonon density as is required for a three-phonon absorption process. ω_R is the longitudinal optical phonon frequency, K is Boltzmann's constant, and T is the absolute temperature. $\overline{B}$ is taken to be a constant that is a measure of the strength of the coupling between the exciton and phonons.

The solid line in Fig. 9 is a best fit of Eq. (24) with $\hbar\Gamma_0 = 1.5\times10^{-4}$ eV and $\hbar\overline{B} = 16\pm3$ eV. It is in fair agreement with the experimental observation which is quite different from the predictions of Toyozawa.[39]

In these experiments carried out at high intensities and at low temperatures, the effects of crystal heating and the possible formation of biexcitons should be considered. An experimental check was made that our observed data on $\chi^{(3)}_{\text{eff}}$ did not depend intrinsically on the laser intensities. Data carried out with the intensity of each of the light beams reduced together or individually by factors of as much as ten yielded the same results at the lowest temperature used. The absorption coefficient at the two-photon resonance, at the highest intensities used in our experiments, is about 0.1 cm^{-1}. The maximum temperature rise above 15 °K consistent with this absorption during the ruby laser pulse is less than 0.25 °K.

If all of the absorbed energy, 0.01 J/g, is assumed to result in the creation of real longitudinal excitons of energy 3.21 eV with lifetimes longer than the laser pulse, the resulting excited exciton density would be at most about $N_E \sim 10^{17}$ cm^{-3}. The ground-state exciton density is 3.8×10^{21} cm^{-1}, and

so only a very small fraction of the excitons undergo a real excitation.

In recent years the study of possible exciton-exciton interactions in CuCl has attracted wide interest.[40-47] However, these effects require exciton densities about two orders of magnitude higher than those achieved in this experiment in order to be seen.

D. Double resonance of longitudinal exciton and phonon polariton

The experimental arrangement with two tunable dye laser beams, described in Sec. III, permits the adjustment of $2\omega_1$ to a value in the vicinity of, or at, the resonance of the longitudinal exciton, and the simultaneous variation of ω_2 so that $\hbar(\omega_1 - \omega_2)$ passes through the longitudinal phonon-polariton resonance at 208 cm^{-1}. Five values for $2\hbar\omega_1$ were chosen: 3.1988 eV, well below the exciton resonance; 3.2083 eV, at the maximum of the exciton resonance; 3.2091 eV, at the location of the minimum in the curve of Fig. 6; 3.2094 eV, just beyond this minimum; and 3.2150 eV, well above the exciton resonance. The signal for $I(2\omega_1 - \omega_2)$ for these five values of ω_1 using the longitudinal orientation is shown in Fig. 10, as $\omega_1 - \omega_2$ is scanned through the infrared polariton resonance. The drawn curves in Fig. 10 represent a best fit to the experimental points based on Eq. (20), to which a background nonresonant two-photon absorption has again been added. The fit was obtained with the following values for the phonon-polariton parameters:

$$\hbar\omega_R = 0.0260(\pm 0.0002)\ \text{eV},$$

$$\hbar\Gamma_R = 3.7\times10^{-4}\ \text{eV},$$

$$4N_R(\alpha_{xyz}^{LR})^2\hbar^2/M_R\chi_{NR}'^{(3)} = 6(\pm 1)\times10^{-6}\ \text{eV}^2.$$

The value $\hbar\omega_R$ agrees quite well with that found from light Raman scattering.[29,48] The damping constant $\hbar\Gamma_R$ has probably not been fully resolved, since the quoted number is only about twice the linewidth of the laser at ω_2. Using known values for the reduced polariton mass M_R, the number density N_R, and the nonresonant susceptibility, the nonlinear phonon-polariton coupling constant obtained is $|\alpha_{xyz}^{LR}| = 1.6(\pm 1)\times10^{-16}$ cm^2. This value is about seven times larger than the corresponding electronic term. Its square is proportional to the spontaneous Raman scattering cross section

$$\sigma_R = \tfrac{64}{3}\pi(\omega_2^4/c^4)(\hbar/M_R\omega_R)|\alpha_{xyz}^{LR}|^2. \qquad (25)$$

Our value for σ_R is about six times smaller than that found by Kaminow and Turner[48] from an absolute measurement of the Raman scattering cross section. The latter is admittedly a very difficult task, and our value of α_{xyz}^{LR}, based on a comparison of nonlinear coefficients, is considered more reliable.

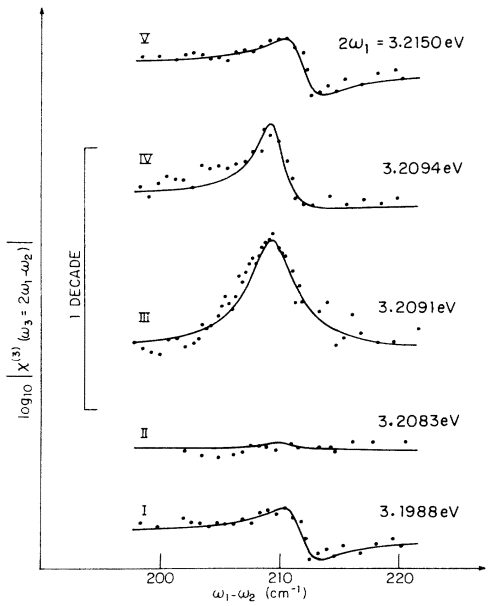

FIG. 10. Dispersion in $|\chi_L^{(3)}(2\omega_1 - \omega_2)|^2$ due to interference between the longitudinal Z_3 exciton polariton and optical phonon polariton in CuCl at 15.1 °K. The labels on the curves indicate the value of the parameter $2\hbar\omega_1$.

The double resonance data of Fig. 10 are displayed in a three-dimensional plot in Fig. 11, where the logarithm of the intensity $I(2\omega_1 - \omega_2)$ is shown as a function of the two frequencies $2\omega_1$ and $\omega_1 - \omega_2$. For $2\omega_1$ either far above or far below the

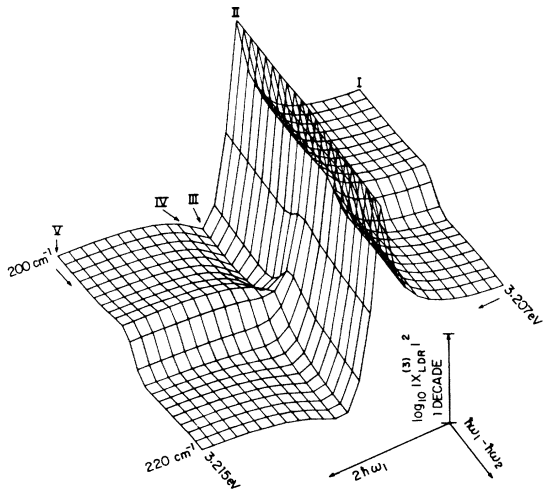

FIG. 11. Three-dimensional plot of the dispersion in $\chi_L^{(3)}(2\omega_1 - \omega_2)$, constructed from the data in Fig. 10.

exciton resonance the curves exhibit the usual interference of a Raman resonant contribution with the nonresonant part of $\chi^{(3)}$. This corresponds to the top and bottom curves in Fig. 10, or cuts I and V in Fig. 11.

The minimum in these curves occurs at the frequency where the real part of the Raman contribution cancels the real part of the effective background susceptibility. As $2\omega_1$ is tuned through the exciton resonance, this background varies dramatically. The location of the minimum is determined by the relative intensities and signs of the Raman and background contributions. For cut II, $2\omega_1$ is exactly at the resonance ω_L. The exciton resonant contribution is so large in Eq. (20) that the variations due to the Raman term are not noticeable. For $2\omega_1$ between the maximum (cut II) and minimum of the exciton curve (cut III), the Raman minimum will be on the low-frequency side of the resonance. This shift in position occurs because the real part of the effective background susceptibility is now negative.

For $2\omega_1$ corresponding to the minimum in the exciton-polariton curve (cut III) the nonresonant and exciton contributions nearly cancel each other in Eq. (20). The magnitude of the mixing signal is now essentially proportional to the absolute square of the Raman phonon-polariton susceptibility alone. This results in a symmetrical curve of $I(2\omega_1 - \omega_2)$ vs $\omega_1 - \omega_2$. Proceeding towards higher values of $2\omega_1$, a continual transition takes place to that of cut V, which shows only the effects of the infrared phonon-polariton resonance. Curve I is virtually identical to curve V in Fig. 10, since the low-frequency exciton contribution to the third-order susceptibility is small compared to the nonresonant part.

V. CONCLUSION

Three-wave mixing techniques supplement the data on linear and nonlinear characteristics of elementary excitations in solids in a significant way. They permit an independent determination of nonlinear coupling constants of exciton and phonon polaritons in CuCl. In addition, the technique has been used to measure the temperature dependence of the longitudinal excitons in the bulk volume of a CuCl crystal for the first time.

The double-resonance data provide a fine example of nonlinear solid-state spectroscopy. While the light beams used and observed all lie in the transparent region of the crystal, the dispersive features associated with the sharp exciton resonance in the ultraviolet and the sharp phonon resonance in the infrared are clearly revealed.

The authors acknowledge many helpful discussions with Dr. Chr. Flytzanis, Dr. F. Parsons, and Dr. E. Yablonovitch. The single crystal of CuCl used in our experiments was kindly provided by Professor H. Mahr. The computer program used to generate Fig. 11 was supplied by R. Lynch, Jr.

---

†Supported by the Joint Services Electronics Program.

*Present address: Oak Ridge National Laboratory, Oak Ridge, Tennessee.

[1]P. D. Maker and R. W. Terhune, Phys. Rev. 137, A801 (1965).

[2]M. D. Levenson and N. Bloembergen, Phys. Rev. B 10, 4447 (1974).

[3]See, for example, Enrico Fermi Course on Nonlinear Spectroscopy, edited by N. Bloembergen (North-Holland, Amsterdam, to to published); *Proceedings of First Taormina Research Conference on the Structure of Matter*, edited by E. Burstein (Pergamon, New York, 1974); *Laser Spectroscopy*, edited by S. Haroche *et al.* (Springer, Berlin, 1975); *Third Conference on the Laser*, edited by L. Goldman in Ann. N. Y. Acad. Sci. 267, 30–60 (1976).

[4]Chr. Flytzanis, in *Quantum Electronics*, edited by H. Rabin and C. L. Tang (Academic, New York, 1975), pp. 9–207, Vol. 1A.

[5]Y. R. Shen, Rev. Mod. Phys. 48, 1 (1976), and numerous references quoted therein.

[6]Chr. Flytzanis and N. Bloembergen, in *Progress in Quantum Electronics*, edited by J. H. Sanders and S. Stenholm (Pergamon, New York, 1976), pp. 271–300, Vol. 4, Pt. 3.

[7]S. D. Kramer, F. G. Parsons, and N. Bloembergen, Phys. Rev. B 9, 1853 (1974); S. D. Kramer and N. Bloembergen, in *Optical Properties of Highly Transparent Solids*, edited by S. S. Mitra and B. Bendow (Plenum, New York, 1975), pp. 365–371.

[8]J. Ringeissen, A. Coret, and S. Nikitine, in *Localized Excitations in Solids*, edited by R. Wallis (Plenum, New York, 1968), p. 297.

[9]S. Nikitine in *Optical Properties of Solids*, edited by S. Nudelman (Plenum, New York, 1969), p. 197.

[10]Y. Kaifu and T. Komatsu, J. Phys. Soc. Jpn. 25, 644 (1968).

[11]A. Feldman and D. Horowitz, J. Opt. Soc. Am. 59, 1406 (1969).

[12]W. Staude, Phys. Lett. A 29, 228 (1969); W. Staude, Phys. Status Solidi 43, 367 (1971).

[13]M. Cardona, Phys. Rev. 129, 69 (1963).

[14]D. C. Haueisen and H. Mahr, Phys. Rev. Lett. 26, 838 (1971); Phys. Rev. B 8, 734 (1973).

[15]J. P. Hermann and J. Ducuing, Phys. Rev. A 5, 2557 (1972).

[16]D. Fröhlich, E. Mohler, and Ch. Uihlein, Phys. Status Solidi 55, 175 (1973).

[17]R. T. Lynch, Jr., S. D. Kramer, H. Lotem, and N. Bloembergen, Opt. Commun. 16, 372 (1976).

[18]S. D. Kramer, Ph.D. thesis (Harvard University, 1976) (unpublished).

[19]D. Boggett and R. Loudon, J. Phys. C 6, 1763 (1973).
[20]D. Boggett and R. Loudon, in *Proceedings of First Taormina Research Conference on the Structure of Matter*, edited by E. Burstein (Pergamon, New York, 1974).
[21]E. Yablonovitch, Chr. Flytzanis, and N. Bloembergen, Phys. Rev. Lett. 29, 865 (1972).
[22]N. Bloembergen and P. S. Pershan, Phys. Rev. 128, 606 (1962).
[23]W. L. Faust and C. H. Henry, Phys. Rev. Lett. 17, 1265 (1966); W. L. Faust, C. H. Henry, and R. H. Eick, Phys. Rev. 173, 781 (1968).
[24]B. F. Levine, Phys. Rev. Lett. 33, 368 (1974).
[25]R. Loudon, in Enrico Fermi Course on Nonlinear Spectroscopy, edited by N. Bloembergen (North-Holland, Amsterdam, to be published); R. Reinisch, N. Paraire, and S. Biraud-Laval, C. R. Acad. Sci. (Paris) 275, 829 (1972).
[26]D. Fröhlich, B. Staginnus, and E. Schönherr, Phys. Rev. Lett. 19, 1032 (1967); D. Fröhlich, E. Mohler, and P. Wiesner, Phys. Rev. Lett. 26, 554 (1971).
[27]R. C. Miller, S. C. Abrahams, R. L. Barns, J. L. Bernstein, W. A. Nordland, and E. H. Turner, Solid State Commun. 9, 1463 (1971). D. Chemla, P. Kupecek, C. Schwartz, C. Schwab, and A. Goltzene, IEEE J. Quantum Electron QE-7, 126 (1971).
[28]D. Bedeaux and N. Bloembergen, Physics 69, 57 (1973).
[29]M. Krauzman, R. M. Pick, H. Poulet, G. Hamel, and B. Prevot, Phys. Rev. Lett. 33, 528 (1974).
[30]Y. Miyazoe and M. Maeda, Appl. Phys. Lett. 12, 206 (1968).
[31]C. F. Dewey, in *Modern Optical Methods in Gas Dynamic Research*, edited by J. Dosanjh (Plenum, New York, 1971), p. 221.
[32]M. Maeda, Japanese Research Institute for Photosensitizing Dyes, Bulletin No. 46 (Okayama, Japan, 1973) (unpublished).
[33]P. P. Sorokin, J. R. Lankard, E. C. Hammond, and V. L. Moruzzi, IBM J. Res. Dev. 11, 130 (1967).
[34]A. Hirth, J. Faure, and D. Lougnot, Optics Commun. 8, 318 (1973).
[35]A. Bivas, C. Marange, J. B. Grun, and C. Schwab, Optics Commun. 6, 142 (1972).
[36]M. Ueta and T. Goto, J. Phys. Soc. Jpn. 20, 401 (1965).
[37]T. Goto, J. Phys. Soc. Jpn. 20, 1654 (1965).
[38]M. Ueta, T. Goto, and T. Yashiro, J. Phys. Soc. Jpn. 20, 1022 (1965).
[39]Y. Toyozawa, Prog. Theor. Phys. 20, 53 (1958).
[40]A. Mysyrowicz, J. B. Grun, R. Levy, A. Bivas, and S. Nikitine, Phys. Lett A 26, 615 (1968).
[41]R. Levy, A. Bivas, and J. B. Grun, Phys. Lett. A 36, 159 (1971).
[42]M. Souma, T. Goto, T. Ohta, and M. Ueta, J. Phys. Soc. Jpn. 29, 697 (1970).
[43]C. Yu, T. Goto, and M. Ueta, J. Phys. Soc. Jpn. 34, 693 (1973).
[44]Y. Kato, T. Goto, T. Fujii, and M. Ueta, J. Phys. Soc. Jpn. 36, 169 (1974).
[45]G. M. Gale and A. Mysyrowicz, Phys. Rev. Lett. 32, 727 (1974).
[46]N. Nagasawa, N. Nakata, Y. Doi, and M. Ueta, J. Phys. Soc. Jpn. 39, 987 (1975).
[47]*Excitons at High Densities*, edited by H. Haken and S. Nikitine (Springer-Verlag, Berlin, 1975).
[48]I. P. Kaminow and E. H. Turner, Phys. Rev. B 5, 1564 (1972).